Genomics Proteomics Bioinformatics 20 (2022) 288–303

Genomics Proteomics Bioinformatics

www.elsevier.com/locate/gpb
www.sciencedirect.com

ORIGINAL RESEARCH

Beneficial Effects of Celastrol on Immune Balance by Modulating Gut Microbiota in Experimental Ulcerative Colitis Mice

Mingyue Li [1,2,#], Weina Guo [1,#], Yalan Dong [1,#], Wenzhu Wang [1,#], Chunxia Tian [1], Zili Zhang [1], Ting Yu [1], Haifeng Zhou [1], Yang Gui [1], Kaming Xue [1], Junyi Li [1], Feng Jiang [3], Alexey Sarapultsev [4], Huafang Wang [5], Ge Zhang [6], Shanshan Luo [5], Heng Fan [1], Desheng Hu [1,*]

[1] *Department of Integrated Traditional Chinese and Western Medicine, Union Hospital, Tongji Medical College, Huazhong University of Science and Technology, Wuhan 430022, China*
[2] *Department of Gastroenterology, Zhongda Hospital, Southeast University, Nanjing 210009, China*
[3] *Institute of International Education, Tianjin University of Traditional Chinese Medicine, Tianjin 301617, China*
[4] *Institute of Immunology and Physiology, Ural Branch of the Russian Academy of Sciences, Ekaterinburg 620049, Russia*
[5] *Institute of Hematology, Union Hospital, Tongji Medical College, Huazhong University of Science and Technology, Wuhan 430022, China*
[6] *Institute of Integrated Bioinfomedicine and Translational Science, School of Chinese Medicine, Hong Kong Baptist University, Hong Kong Special Administrative Region 999077, China*

Received 5 March 2021; revised 27 April 2022; accepted 11 May 2022
Available online 21 May 2022

Handled by Jingyuan Fu

KEYWORDS

Ulcerative colitis;
Celastrol;
Gut microbiota;
Treg/Th balance;
Metabolomics

Abstract **Ulcerative colitis** (UC) is a chronic inflammatory bowel disease caused by many factors including colonic inflammation and microbiota dysbiosis. Previous studies have indicated that **celastrol** (CSR) has strong anti-inflammatory and immune-inhibitory effects. Here, we investigated the effects of CSR on colonic inflammation and mucosal immunity in an experimental colitis model, and addressed the mechanism by which CSR exerts the protective effects. We characterized the therapeutic effects and the potential mechanism of CSR on treating UC using histological staining, intestinal permeability assay, cytokine assay, flow cytometry, fecal microbiota transplantation (FMT), 16S rRNA sequencing, untargeted **metabolomics**, and cell differentiation. CSR administration significantly ameliorated the dextran sodium sulfate (DSS)-induced colitis in mice, which was

* Corresponding author.
E-mail: desheng.hu@hust.edu.cn (Hu D).
# Equal contribution.

Peer review under responsibility of Beijing Institute of Genomics, Chinese Academy of Sciences / China National Center for Bioinformation and Genetics Society of China.

https://doi.org/10.1016/j.gpb.2022.05.002

evidenced by the recovered body weight and colon length as well as the decreased disease activity index (DAI) score and intestinal permeability. Meanwhile, CSR down-regulated the production of pro-inflammatory cytokines and up-regulated the amount of anti-inflammatory mediators at both mRNA and protein levels, and improved the balances of Treg/Th1 and Treg/Th17 to maintain the colonic immune homeostasis. Notably, all the therapeutic effects were exerted in a **gut microbiota**-dependent manner. Furthermore, CSR treatment increased the gut microbiota diversity and changed the compositions of the gut microbiota and metabolites, which is probably associated with the gut microbiota-mediated protective effects. In conclusion, this study provides the strong evidence that CSR may be a promising therapeutic drug for UC.

Introduction

Ulcerative colitis (UC) is one of the two major forms of inflammatory bowel diseases (IBDs), which is featured with diffuse inflammation in the colonic mucosa. With the poor life quality and the high morbidity and risk of colitis-related colorectal cancer, UC has become a public health threat [1,2]. The current treatment strategies for UC include oral and/or topical 5-aminosalicylic acid, local and systemic corticosteroids, and a combined therapy with anti-tumor necrosis factor (TNF) and immunomodulator, depending on the severity, distribution, and pattern of the disease. Among these treatment strategies, 5-aminosalicylic acid is the recommended first-line medication for induction and maintenance therapy [3,4]. Due to the low remission rate of new drugs or the secondary loss of therapeutic effects, the majority of patients unresponsive to these therapies will eventually undergo surgery [5].

The pathogenesis of UC still remains unclear. Several factors, including the genetic susceptibility, dysregulated immune responses, imbalanced gut microbiota, and environmental exposure, have been reported to be implicated [6]. The imbalance between T helper (Th) cells and regulatory T (Treg) cells has been proven to be correlated with the occurrence and severity of UC [7]. During UC progression, Th1 and Th17 cells are usually accumulating and exerting pathogenic effects by releasing the pro-inflammatory cytokines including interferon-γ (IFN-γ) and interleukin-17A (IL-17A), respectively. While Treg cells are down-regulated, which inhibit the activities of Th1 and Th17 cells through intercellular communication [8–13].

It has been strongly implicated that in addition to the gut microbiota-derived signals, the composition and function of gut microbiota have been altered markedly in patients with UC [14]. The gut microbiota and its metabolites exert bidirectional effects on each other. Dysbiosis of gut microbiota is able to skew the balance of Treg/Th17 cells, trigger exaggerated inflammatory responses, and alter the gut microbiota-derived metabolites in UC [15]. The gut microbiota-derived metabolites exert important and diverse effects on host physiology and are detectable in a wide range of biological tissues [15–17]. The reduction of several gut microbiota-derived metabolite classes is the focus of severe inflammation as well as UC, of which the prominent members are short-chain fatty acids (SCFAs), bile acid derivatives, and tryptophan metabolites [14]. The metabolites are reported to be protective in colitis through expanding the pool of intestinal Treg cell [18], producing antimicrobial peptides [19,20], and maintaining the mucosal immunity and homeostasis [21,22]. Therefore, maintaining the homeostasis of gut microbiota might be a promising therapeutic strategy for UC.

Celastrol (CSR) is the major component of a herb used in Traditional Chinese Medicine for several centuries, which is isolated from the root xylem of *Tripterygium wilfordii*. With strong antioxidant, anti-inflammatory, and anti-cancer properties, accumulating evidence has indicated the medicinal usefulness of CSR in disparate clinical fields, including rheumatoid arthritis, IBDs, systemic lupus erythematosus, osteoarthritis, and allergy, as well as cancer and neurodegenerative disorders [23]. In the mouse model of dextran sodium sulfate (DSS)-induced colitis, the results have revealed that CSR ameliorates acute intestinal injury and prevents the loss of intestinal epithelial homeostasis via suppressing colonic oxidative stress, inhibiting NLRP3 inflammasome and IL-23/IL-17 pathway, reducing inflammatory cytokines, attenuating neutrophil infiltration, and up-regulating E-cadherin expression [24,25].

However, the intrinsic therapeutic mechanism of CSR on UC still needs to be clarified. Given the vital role of gut microbiota dysbiosis and immune dysregulation in the pathogenesis of UC, we sought to address the potential impacts of CSR on gut micro-ecosystem and immune system in DSS-induced colitis in mouse model.

Results

CSR administration ameliorates DSS-induced colitis

To investigate the therapeutic effects of CSR (Figure S1A) on UC, DSS-induced colitis model was established in this study. Mice were treated with 3.0% DSS in the drinking water, and CSR suspended in saline was administered by oral gavage for 7 days (**Figure 1**A). Compared to the DSS+ group, CSR administration ameliorated DSS-induced colitis in the DSS+CSR+ group, as evidenced by the remarkably reduced body weight loss (Figure 1B), and improved colon length (Figure 1C). Furthermore, the disease activity index (DAI) score based on the assessment of stool consistency, bloody stool, and weight loss was concord with the aforementioned results, validating the curative effect of CSR on UC (Figure 1D). To test the intestinal permeability, the mice were gavaged with fluorescein isothiocyanate conjugated dextran (FITC-dextran) 4 h before being euthanized. Compared to the DSS+ group, mice in the DSS+CSR+ group exhibited a decreased serum level of FITC-dextran, indicating the relatively intact epithelial barrier (Figure 1E). Additionally, hematoxylin and eosin (H&E) staining was performed to evaluate the extent of colon injuries. Compared to DSS-induced colitis in the mice of the DSS+ group, the distorted crypts, lost goblet cells, epithelial injury, and the infiltrating inflammatory cells in the mucosa and submucosa were remarkably alleviated in the mice of the

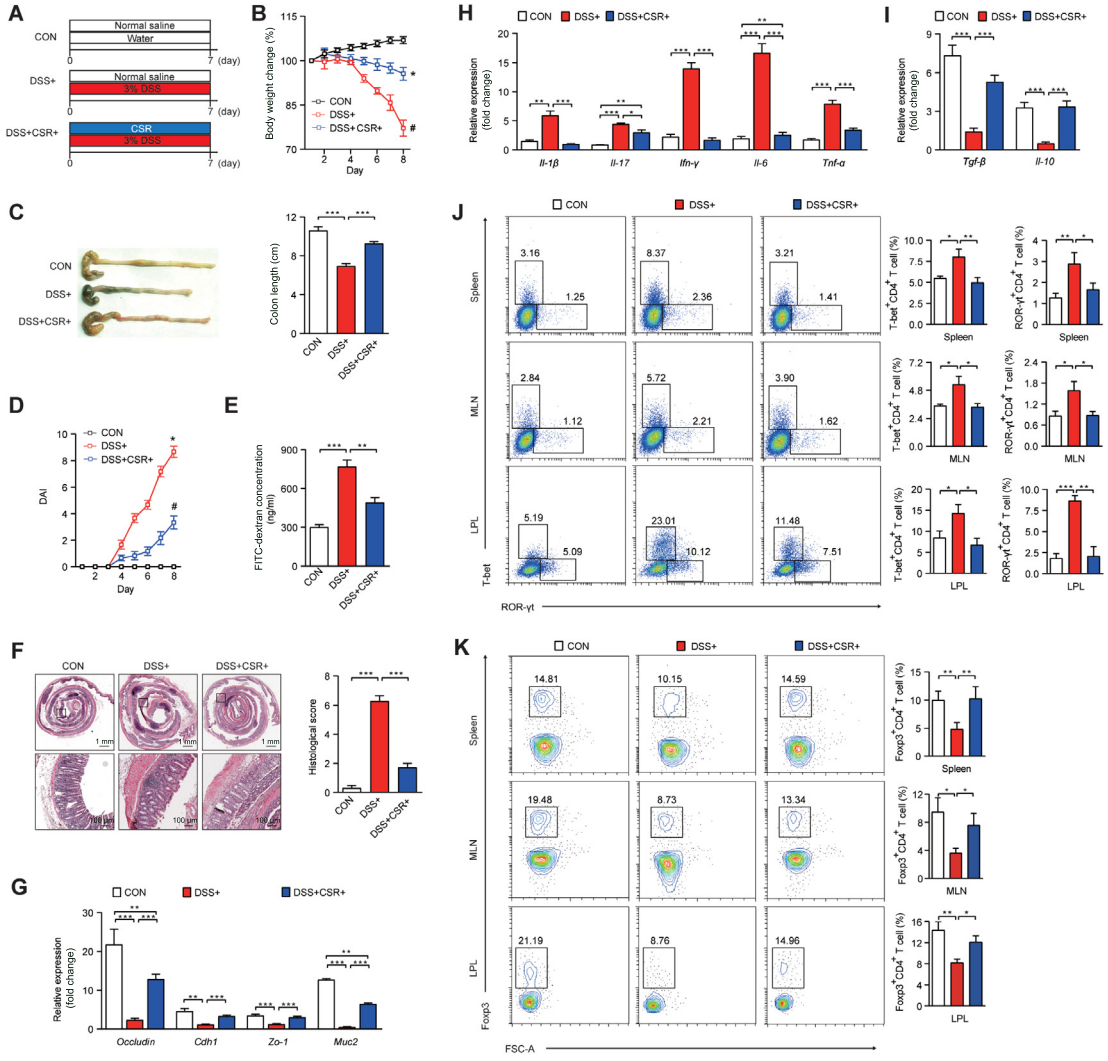

Figure 1 CSR attenuates DSS-induced experimental colitis in mice

A. Schematic diagram illustrating the experimental design. **B.** Body weight change of each group (n = 10). **C.** Measurement of the length of colons harvested from mice in each group (n = 10). **D.** The effect of CSR on DAI of mice in each group (n = 10). **E.** Mice in each group received an oral gavage of FITC-dextran (0.5 mg/g) and the serum FITC-dextran concentration was determined 4 h later (n = 5). **F.** H&E staining sections and histological scores of colon tissues from mice in each group (n = 5). Scale bars, 1 mm (top) and 100 μm (bottom). **G.** The expression levels of *Occludin*, *Cdh1*, *Zo-1*, and *Muc2* in colon tissues from mice in each group (n = 5). **H.** The expression levels of pro-inflammatory cytokine genes in colon tissues from mice in each group (n = 5). **I.** The expression levels of anti-inflammatory cytokine genes in colon tissues from mice in each group (n = 5). **J.** T-bet$^+$CD4$^+$ (Th1) cells and ROR-γt$^+$CD4$^+$ (Th17) cells in the spleen, MLN, and LPL of mice from the control, DSS+, and DSS+CSR+ groups were analyzed by flow cytometry and their percentages were shown in the bar charts (n = 5). **K.** Foxp3$^+$CD4$^+$ (Treg) cells in the spleen, MLN, and LPL of mice from the control, DSS+, and DSS+CSR+ groups were analyzed by flow cytometry and their percentages were shown in the bar charts (n = 5). Data were presented as mean ± SEM. The one-way ANOVA with Tukey's test was applied to test the significant differences among different groups. *, $P < 0.05$; **, $P < 0.01$; ***, $P < 0.001$. CON, control; CSR, celastrol; DSS, dextran sodium sulfate; DAI, disease activity index; FITC, fluorescein isothiocyanate; H&E, hematoxylin and eosin; MLN, mesenteric lymph node; LPL, lamina propria lymphocyte; SEM, standard error of the mean; ANOVA, analysis of variance; FDS-A, forward scatter-area.

DSS+CSR+ group. These phenomena indicated that CSR controlled colon inflammation and maintained epithelial barrier integrity well (Figure 1F), which was further confirmed by Alcian blue staining revealing the intensity of goblet cells (Figure S1B). Since tight junction plays a vital role in maintaining the barrier of epithelia in colon, we next assessed the expression of tight junction-related genes/proteins. Data revealed that DSS up-regulated the expression of Claudin2, inhibited the expression of *Occludin*, *Cdh1*, *Zo-1*, and *Muc2*, which were rescued by CSR treatment (Figure 1G, Figure S1C). Immune cells and the secreted inflammatory cytokines are important mediators for immune homeostasis in the gut. Hence, we examined these mediators in the colon tissues. The pro-inflammatory cytokine genes, including *Il-1β*, *Il-17a*, *Ifn-γ*, *Il-6*, and *Tnf-α*, and the proteins such as IFN-γ and TNF-α in colon were down-regulated, while the

anti-inflammatory cytokine genes *Tgf-β* and *Il-10* were up-regulated in colon tissues of mice in the DSS+CSR+ group (Figure 1H and I, Figure S1C). The frequencies of IFN-γ^+CD4$^+$ and IL-17A$^+$CD4$^+$ T cells in the spleen and mesenteric lymph node (MLN) in DSS+CSR+ group were reduced (Figure S1D). Meanwhile, the percentages of T-bet$^+$CD4$^+$ and ROR-γt$^+$CD4$^+$ T cells in the spleen, MLN, and colonic lamina propria lymphocyte (LPL), were down-regulated, while the percentages of Foxp3$^+$CD4$^+$ T cells were up-regulated in the spleen, MLN, and colonic LPL of mice in the DSS+CSR+ group (Figure 1J and K).

Paneth cells are an important source of antimicrobial peptides in the intestine which secrete several antimicrobial peptides, such as Lysozyme, RegIII, cryptdin4, and cryptdin5. qRT-PCR was performed to test the expression of the antimicrobial peptides. And the results showed that the levels of these antimicrobial peptides were up-regulated in both the DSS+ and DSS+CSR+ groups. In addition, the mRNA level of RegIII in the DSS+ group was higher than that in the DSS+CSR+ group (Figure S1E). Together, these results indicate that CSR can prevent DSS-induced colitis.

CSR promotes the differentiation of Treg cells *in vitro*

To further explore whether CSR directly regulates T cell differentiation, naive CD4$^+$ T cells were isolated from the spleen of the wild-type (WT) mice and co-cultured with different concentrations of CSR under the corresponding conditions for Th1, Th17, and Treg cell differentiation *in vitro*. The results showed that CSR had no effect on the differentiation of IFN-γ^+CD4$^+$ T cells and IL-17A$^+$CD4$^+$ T cells in the indicated CSR concentrations. However, Foxp3$^+$CD4$^+$ T cells were elevated when the concentration of CSR was 4 μM (Figure S2).

CSR alleviates colitis in a gut microbiota-dependent manner

To investigate whether gut microbiota mediates the protective effects of CSR on DSS-induced colitis, the WT mice were treated with quadruple antibiotic cocktail (ABX) for gut microbiota depletion before DSS treatment (**Figure 2**A). Following the 3-week ABX treatment, the gut microbiota including Eubacteria, *Lactobacillus*, mouse intestinal *Bacteroides* (MIB), and *Eubacterium* rectale-*Clostridium* coccoides were significantly decreased in the fecal samples of ABX-treated mice compared to those of the untreated mice (Figure S3A), which was consistent with the previous research [26]. Moreover, there was no difference in the morphology of liver, kidney, intestine, and colon, and the serum levels of alanine aminotransferase (ALT), aspartate aminotransferase (AST), blood urea nitrogen (BUN), and creatinine (CRE) after ABX treatment compared to the untreated mice, indicating the non-organ toxicity of ABX treatment (Figure S3B and C). Impressively, the therapeutic effects of CSR were disappeared after gut microbiota depletion. The mice in the ABX+DSS+ group and those in the ABX+DSS+CSR+ group displayed no significant difference in the following indices: body weight (Figure 2B), colon length (Figure 2C), DAI score (Figure 2D), intestinal permeability (Figure 2E), histological changes and scores (Figure 2F), the intensity of goblet cells (Figure S4A), the expression levels of tight junction-related genes/proteins (Figure 2G, Figure S4B), the expression levels of pro-inflammatory cytokine genes (Figure 2H), and the expression levels of anti-inflammatory cytokine genes (Figure 2I). In addition, the percentages of T-bet$^+$CD4$^+$, ROR-γt$^+$CD4$^+$, and Foxp3$^+$CD4$^+$ T cells in the spleen, MLN, and colonic LPL (Figure 2J and K), as well as the percentages of IFN-γ^+CD4$^+$ and IL-17A$^+$CD4$^+$ T cells in the spleen and MLN (Figure S4C), showed no significant difference between the ABX+DSS+ group and ABX+DSS+CSR+ group. These results demonstrate that the protective effects of CSR on colitis is gut microbiota-dependent.

Fecal microbiota transplantation mitigates colitis

To gain deeper insight into the protective effects of CSR about how it regulates the gut microbiota, we conducted a fecal microbiota transplantation (FMT) experiment. Fecal microbiota from the mice of the DSS−CSR−, DSS+CSR− and DSS+CSR+ groups were transferred into DSS-induced colitic mice, respectively (**Figure 3**A). Compared to the mice with FMT from the DSS−CSR− group, the mice with FMT from the DSS+CSR− group showed the more serious weight loss (Figure 3B) and colon shortening (Figure 3C), higher DAI score (Figure 3D), higher intestinal permeability (Figure 3E), higher histology score (Figure 3F), less goblet cells (Figure S5A), and lower expression levels of tight junction-related genes/proteins (Figure 3G, Figure S5B), which were completely reversed in the mice with FMT from the DSS+CSR+ group. Representative microscopic H&E staining and Alcian blue staining pictures are shown in Figure 3F and Figure S5A. Furthermore, compared to the mice with FMT from the DSS−CSR− group, the frequencies of Th1 and Th17 cells and the expression levels of pro-inflammatory cytokine genes were increased, while the expression levels of anti-inflammatory cytokine genes were decreased in the mice with FMT from the DSS+CSR− group. Again, all the aforementioned disease-modifying tendencies were reversed in the mice with FMT from the DSS+CSR+ group (Figure 3H–K, Figure S5B and C). These FMT results indicate that gut microbiota in mice from the DSS+CSR+ group is responsible for the alleviated colitis.

CSR significantly influences the gut microbiota

It has been reported that gut microbiota plays important roles in maintaining intestinal homeostasis and T cell functions. High-throughput sequencing analysis of the 16S rRNA gene in fecal bacterial DNA isolated from the mice in the control, DSS+, and DSS+CSR+ groups was performed to investigate whether CSR alters gut microbiome. We initially measured the gut microbial alpha diversity through different indices, including observed species, Chao, ace, and PD_whole tree indices, and found that, compared to the DSS+ group, the mice in the DSS+CSR+ group harbored a microbiota with higher alpha diversity (**Figure 4**A). To further explore the diversity of the gut microbiota, we measured the beta diversity and then performed a principal coordinate analysis (PCoA) using the binary-jaccard distance and unweighted-unifrac distance algorithms. The obvious clustering separation between operational taxonomic units (OTUs) reveals the different community structures among the three groups, indicating that these

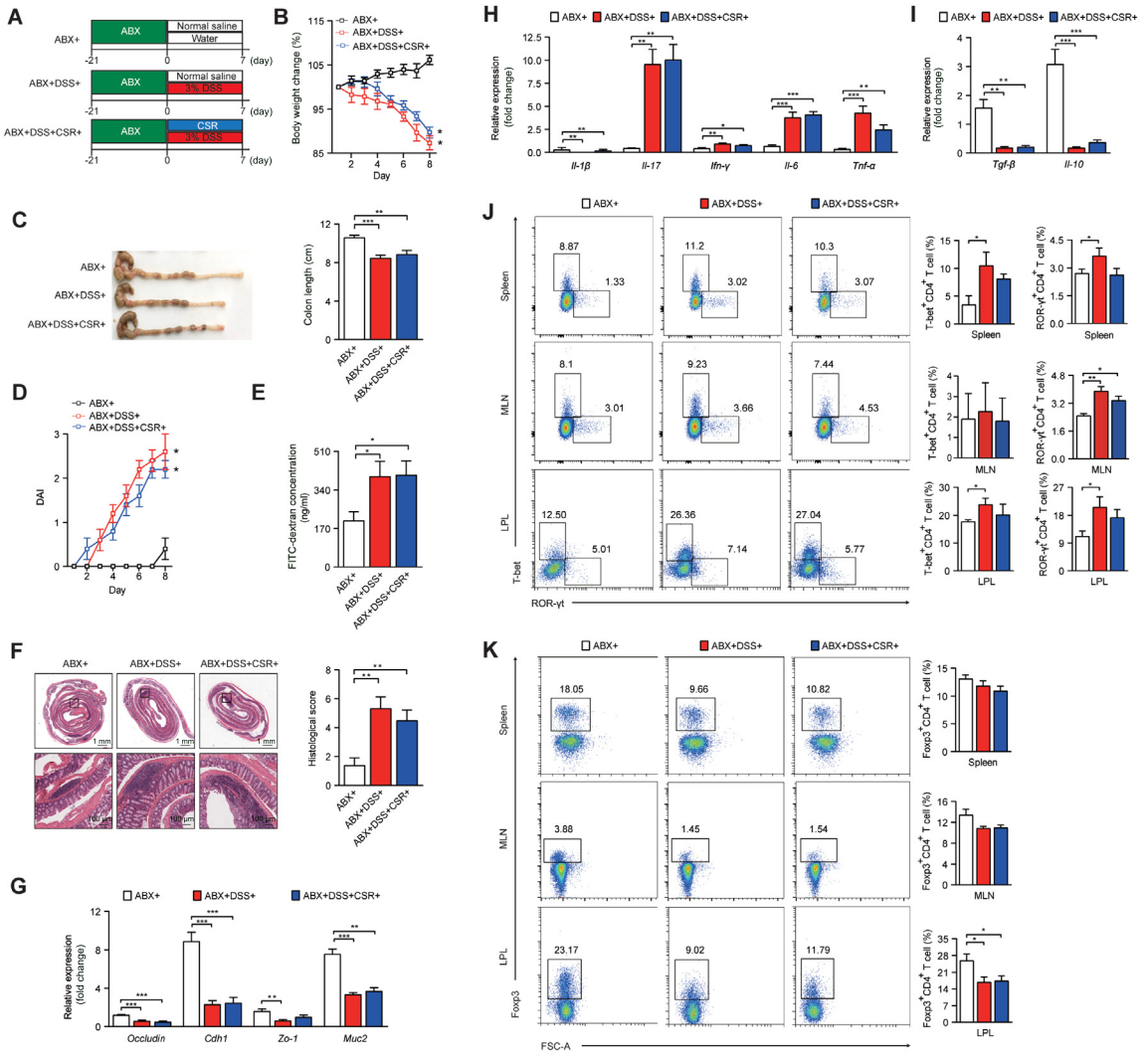

Figure 2 Effects of CSR on DSS-induced colitis after pretreatment with ABX

A. Schematic diagram illustrating the experimental design. **B.** Body weight change of each group (n = 10). **C.** Measurement of the length of colons harvested from mice in each group (n = 10). **D.** The effect of CSR on DAI of mice in each group (n = 10). **E.** Mice in each group received an oral gavage of FITC-dextran (0.5 mg/g) and the serum FITC-dextran concentration was determined 4 h later (n = 5). **F.** H&E staining sections and histological scores of colon tissues from mice in each group (n = 5). Scale bars, 1 mm (top) and 100 μm (bottom). **G.** The expression levels of *Occludin*, *Cdh1*, *Zo-1*, and *Muc2* in colon tissues from mice in each group (n = 5). **H.** The expression levels of pro-inflammatory cytokine genes in colon tissues from mice in each group (n = 5). **I.** The expression levels of anti-inflammatory cytokine genes in colon tissues from mice in each group (n = 5). **J.** T-bet$^+$CD4$^+$ (Th1) cells and ROR-γt$^+$CD4$^+$ (Th17) cells in the spleen, MLN, and LPL of mice from the ABX+, ABX+DSS+, and ABX+DSS+CSR+ groups were analyzed by flow cytometry and their percentages were shown in the bar charts (n = 5). **K.** Foxp3$^+$CD4$^+$ (Treg) cells in the spleen, MLN, and LPL of mice from the ABX+, ABX+DSS+, and ABX+DSS+CSR+ groups were analyzed by flow cytometry and their percentages were shown in the bar charts (n = 5). Data were presented as mean ± SEM. The one-way ANOVA with Tukey's test was applied to test the significant differences among different groups. *, $P < 0.05$; **, $P < 0.01$; ***, $P < 0.001$. ABX, antibiotic cocktail.

communities are different in composition and structure (Figure 4B).

Subsequently, we evaluated the gut microbiota in all samples to find possible compositional differences among the three groups. At the phylum level, the most abundant phyla were Bacteroidetes and Firmicutes in all samples. Additionally, the ratio of Firmicutes to Bacteroidetes (F/B) showed no significant difference among the three groups (Figure S6A). Taxonomic compositions of the three groups were also compared at the class/order/family level (Figure S6B–D). At the genus level, the three groups displayed obviously differential taxonomic compositions (Figure S6E). The differential bacterial genera with higher relative abundance in three groups were analyzed. *Alloprevotella* and *Odoribacter* displayed relatively higher abundance in the DSS+ and DSS+CSR+ groups, whereas the *unidentified_Lachnospiraceae* was more abundant in the control group (Figure S6F).

To confirm which bacteria were changed by CSR treatment, we conducted high-dimensional class comparisons using the linear discriminant analysis (LDA) of effect size (LEfSe),

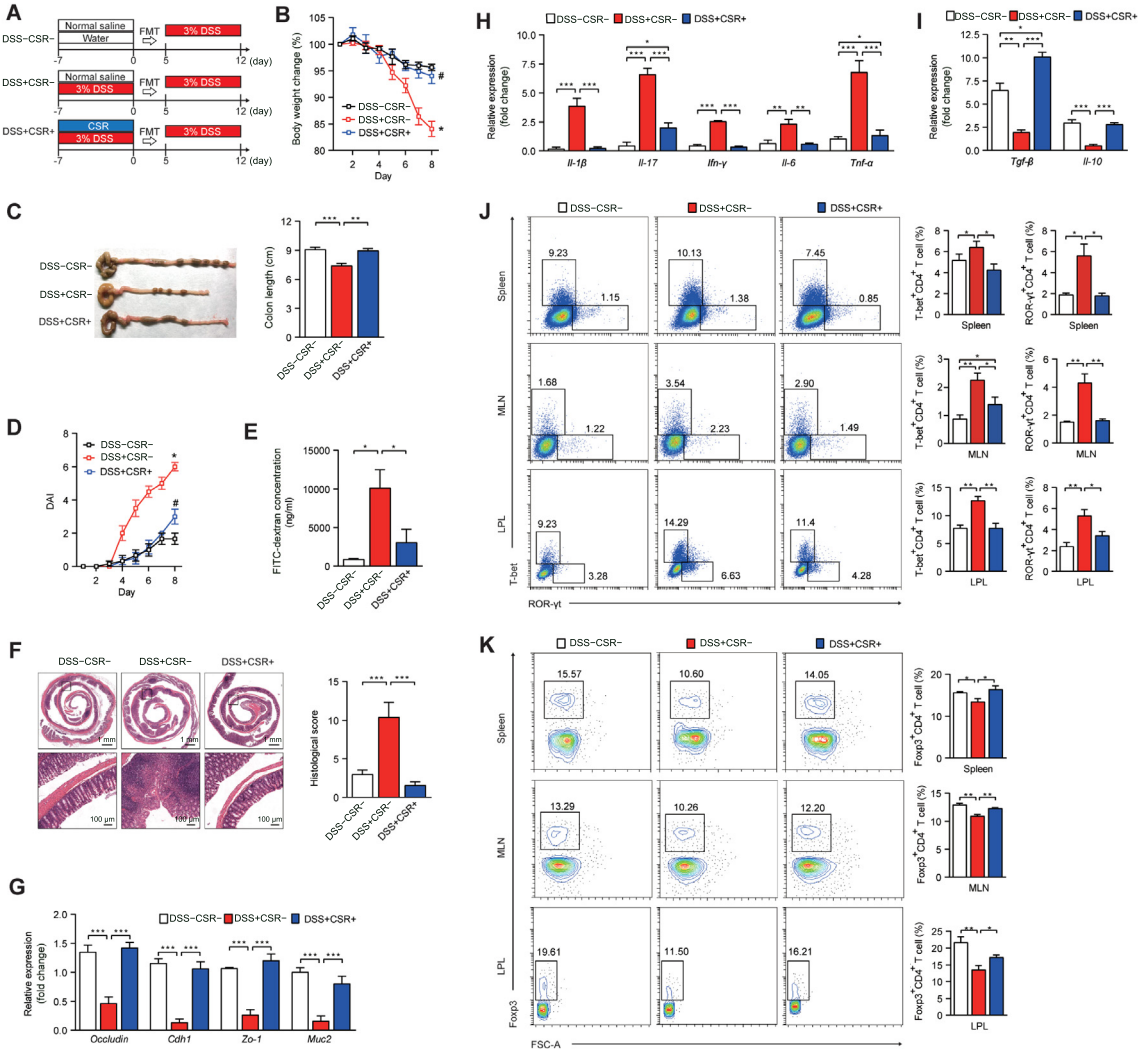

Figure 3 Fecal transplants from CSR-treated mice confer the protection for colitic mice

A. Schematic diagram illustrating the experimental design. **B.** Body weight change of each group (n = 10). **C.** Measurement of the length of colons harvested from mice in each group (n = 10). **D.** The effect of CSR on DAI of mice in each group (n = 10). **E.** Mice in each group received an oral gavage of FITC-dextran (0.5 mg/g) and the serum FITC-dextran concentration was determined 4 h later (n = 5). **F.** H&E staining sections and histological scores of colon tissues from mice in each group (n = 5). Scale bars, 1 mm (top) and 100 μm (bottom). **G.** The expression levels of *Occludin*, *Cdh1*, *Zo-1*, and *Muc2* in colon tissues from mice in each group (n = 5). **H.** The expression levels of pro-inflammatory cytokine genes in colon tissues from mice in each group (n = 5). **I.** The expression levels of anti-inflammatory cytokine genes in colon tissues from mice in each group (n = 5). **J.** T-bet$^+$CD4$^+$ (Th1) cells and ROR-γt$^+$CD4$^+$ (Th17) cells in the spleen, MLN, and LPL from mice with FMT from the DSS−CSR−, DSS+CSR−, and DSS+CSR+ groups were analyzed by flow cytometry and their percentages were shown in the bar charts (n = 5). **K.** Foxp3$^+$CD4$^+$ (Treg) cells in the spleen, MLN, and LPL from mice with FMT from the DSS−CSR−, DSS+CSR−, and DSS+CSR+ groups were analyzed by flow cytometry and their percentages were shown in the bar charts (n = 5). Data were presented as mean ± SEM. The one-way ANOVA with Tukey's test was applied to test the significant differences among different groups. *, $P < 0.05$; **, $P < 0.01$; ***, $P < 0.001$. FMT, fecal microbiota transplantation.

and looked for differences in the predominance of bacterial communities among the three groups (Figure 4C and D). The results showed that *Odoribacter* and Marinifilaceae were the key types of bacteria resulting in the gut microbiota dysbiosis in the DSS-induced colitic mice. However, *Prevotellaceae*, *Alloprevotella*, *Paraprevotella*, and *Butyricicoccus* displayed a relative enrichment in the DSS+CSR+ group, which might be associated with the CSR-mediated alleviation of colitis. Based on the OTU abundance at the genus level, the inter-group difference of gut microbiota among the three groups was shown in the comparison heatmap (Figure 4E). Similarly, the genera *Alloprevotella* and *Butyricicoccus* displayed a relatively higher abundance in the DSS+CSR+ group, while the genus *Odoribacter* was significantly enriched in the DSS+ group, which was consistent with the LEfSe results. In conclusion, CSR treatment significantly alters the gut microbiota diversity and composition.

Next, we compared the gut microbiomes between mice from the DSS−CSR− and DSS−CSR+ groups. We measured the gut microbial alpha diversity through different indices,

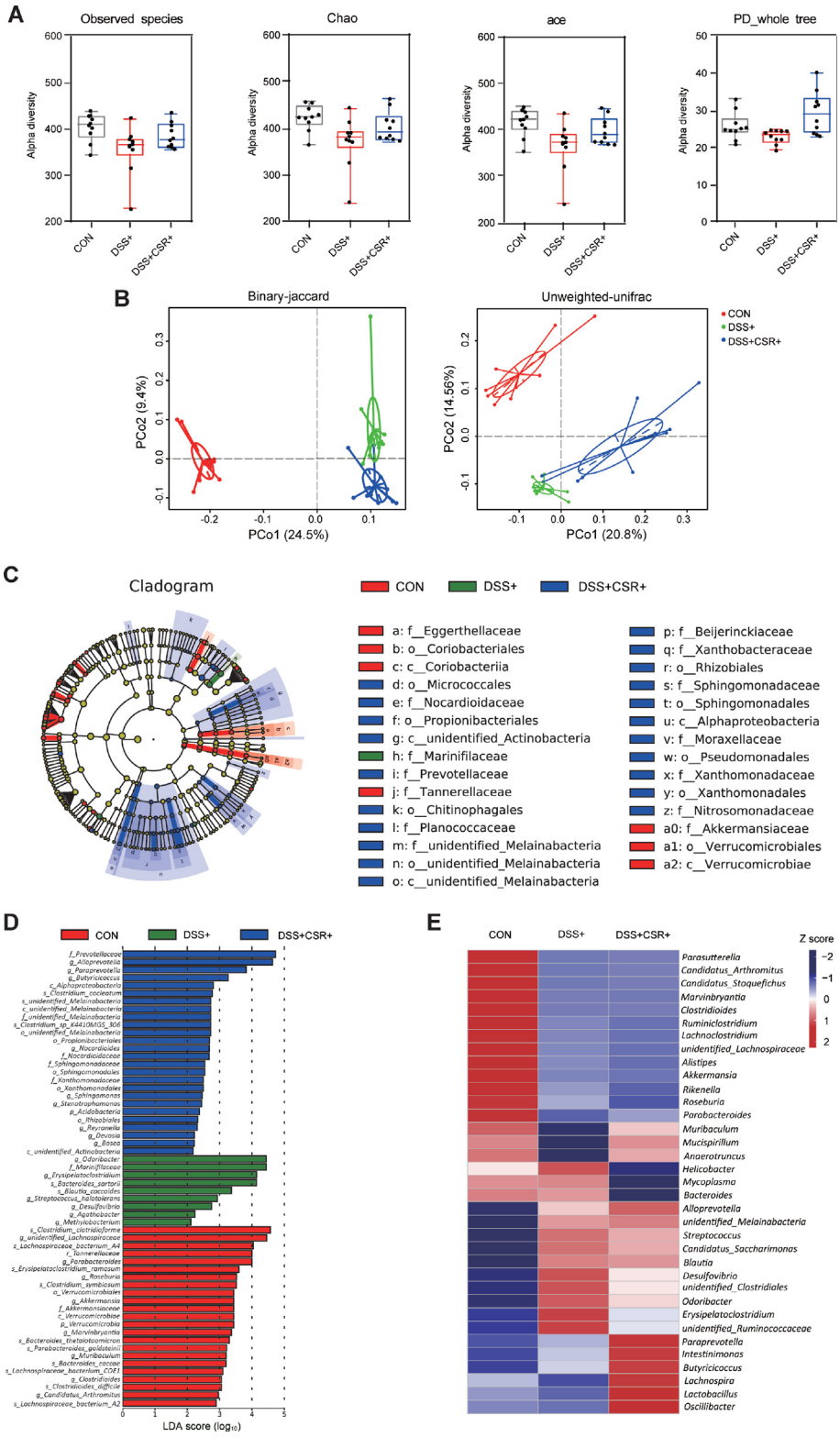

Figure 4 CSR treatment significantly alters the gut microbiota diversity and composition

A. Alpha diversity boxplot (observed species, Chao, ace, and PD_whole tree). **B.** PCoA using binary-jaccard and unweighted-uniFrac of beta diversity. **C.** Taxonomic cladogram from LEfSe, depicting taxonomic association between microbiota communities from the control, DSS+, and DSS+CSR+ groups. **D.** LDA score computed from features differently abundant among the control, DSS+, and DSS+CSR+ groups. **E.** Heatmap of selected most differently abundant features at the genus level. Blue represents less abundant, white represents intermediate abundance, and red represents the most abundant. Each block represents an individual mouse. PCoA, principal coordinate analysis; LDA, linear discriminant analysis; PCo, principal coordinate; LEfSe, linear discriminant analysis of effect size.

including observed species, Chao, PD_whole tree, and Simpson, and found that mice in the DSS−CSR+ group harbored a microbiota with higher alpha diversity than that of the DSS−CSR− group (Figure S7A). Unweighted-unifrac, unweighted-*t*_test, and unweighted-two_wilcox were used to measure the gut microbial beta diversity. The results showed that the DSS−CSR+ group harbored a microbiota with significantly higher beta diversity than that of the DSS−CSR− group (Figure S7B). To further explore the diversity of the gut microbiota, we performed a PCoA using the unweighted-unifrac distance of beta diversity. The clustering separation between OTUs revealed the different community structures of the two groups (Figure S7C). Based on the OTU abundance at the genus level, the inter-group difference of gut microbiota among the two groups was shown in the comparison heatmap (Figure S7D). Similar to the DSS+CSR+ group, the genera *Alloprevotella* and *Prevotellaceae* displayed a relatively higher abundance in the DSS−CSR+ group, which might be associated with the CSR-mediated alleviation of colitis.

CSR significantly alters gut metabolome

Metabolites are the major executors of gut microbiota in the pathogenesis of inflammatory diseases [27]. Hence, to address the role of CSR in affecting gut metabolites, we performed non-target metabolomics analysis on the isolated feces of mice from the DSS+ group and the DSS+CSR+ group. Partial least-squares discrimination analysis (PLS-DA) and hierarchical clustering revealed that the metabolomic profile of the DSS+CSR+ mice was remarkably different from that of the DSS+ mice (**Figure 5**A and B). Under both the negative and positive ion modes, a total of 24 metabolites were more abundant in the DSS+CSR+ mice than in the DSS+ mice (Figure 5C and D). Then the influences of these metabolites on the differentiation of naive $CD4^+$ T cells were explored *in vitro*, and we found that pyruvate and adenosine showed their potential functions. In details, pyruvate down-regulated the differentiation of IFN-γ^+CD4^+ T cells and IL-$17A^+CD4^+$ T cells (**Figure 6**A and B), and adenosine up-regulated the differentiation of $Foxp3^+CD4^+$ T cells *in vitro* (Figure 6C). In summary, CSR administration obviously alters the metabolome in colon, which in turn affects the differentiation of naive T cells.

Furthermore, metabolites in mice from the DSS−CSR− and DSS−CSR+ groups were measured. PLS-DA and hierarchical clustering revealed that the metabolomic profile of the DSS−CSR+ group was significantly different from that of the DSS−CSR− group (Figures S8A and B). Under both the negative and positive ion modes, a total of 46 metabolites were more abundant in the DSS−CSR+ group than in the DSS−CSR− group. However, these differential metabolites were not completely consistent with those identified between the DSS+ and DSS+CSR+ groups. According to the aforementioned results, CSR indeed alters the compositions of the gut microbiota and metabolites directly. However, it is also possible that the alleviation of colitis may play a certain regulatory role on the gut microbiota and metabolites.

Discussion

UC is a subtype of IBDs, which is characterized by chronic recurrent inflammation of the colonic mucosa. The clinical manifestations are recurrent abdominal pain, and loose and bloody stools. Currently, drugs applied in the treatment are challenged by insufficient effects, drug dependence, adverse reactions, and high costs. Thus, it is worthy of in-depth investigation to find new UC therapies with better performance. CSR, with prominent anti-inflammatory and antioxidant effects, is anticipated to be an effective element in *Tripterygium wilfordii*, which has been "clinically" tested in the Traditional Chinese Medicine for thousand years. In this study, we systematically studied the therapeutic effects of CSR on DSS-induced colitis in mice and its potential mechanism (**Figure 7**).

The symptom of DSS-induced colitis in mice is similar to that of human UC, and the DSS-induced colitis model is a well-acknowledged and widely-used animal model for studying UC currently [28]. DSS-induced colitis in mice reveals the typical UC features, including inflammation that starts from the distal colon and then involves in the proximal colon, body weight loss, shortening of colon length, mucosal ulcers, and infiltration of inflammatory granulocytes [29]. In this study, we found that CSR significantly affected the intensity of intestinal inflammation and reversed the imbalances of Treg/Th17 and Treg/Th1 in the intestinal mucosa. These results are similar to those reported in previous studies, where the beneficial effects of CSR on the Th17/Treg cell-mediated responses have been revealed in the animal models of autoimmune arthritis and autoimmune encephalomyelitis [30,31].

Gut microbiota dysbiosis plays a vital role in the pathogenesis of UC [32,33], and various therapeutic microbial manipulations (such as antibiotics, probiotics, prebiotics, and microbiota transplantation) have been proved to be a promising treatment strategy [34–36]. To reveal the underlying therapeutic mechanism of CSR, we investigated whether gut microbiota contributes to its protective effects. Notably, there was no significant difference in the severity of colon inflammation between the ABX+DSS+ group and the ABX+DSS+CSR+ group, indicating that the protective effects of CSR disappear after depleting gut microbiota. Subsequently, we conducted FMT to explore whether the protective effects of CSR are attributed to gut microbiota and are transferable. In contrast to the feces from the DSS+CSR− mice, the feces from the DSS+CSR+ mice alleviated the inflammatory response and rectified the imbalances of Treg/Th1 and Treg/Th17 in DSS-induced colitic mice. The *in vitro* experiments confirmed that, without the participation of gut microbiota, CSR indeed lost its role in regulating the differentiation of Th1, Th17, and Treg cells. Therefore, the immune-mediating action of CSR is due to its influence on the gut microbiota.

According to the literature, UC patients show a decrease in the biological diversity of gut microbiota composition, which is called dysbiosis and characterized by the loss of beneficial bacteria and the expansion of pathogenic bacteria [15]. For instance, the relative abundances of beneficial bacterial species in UC patients, such as *Prevotella copri* and the butyrate-producing bacterium *Faecalibacterium prauznitzii*, have been shown to decrease remarkably. In this study, to further clarify the influence of CSR on the structure and composition of gut microbiota, the 16S rRNA sequencing was conducted. The alpha diversity indices, including observed species, Chao, ace, and PD_whole tree, revealed that the mice in the DSS+CSR+ group harbored a higher diversity than those in the DSS+ group. The beta diversity analysis revealed that

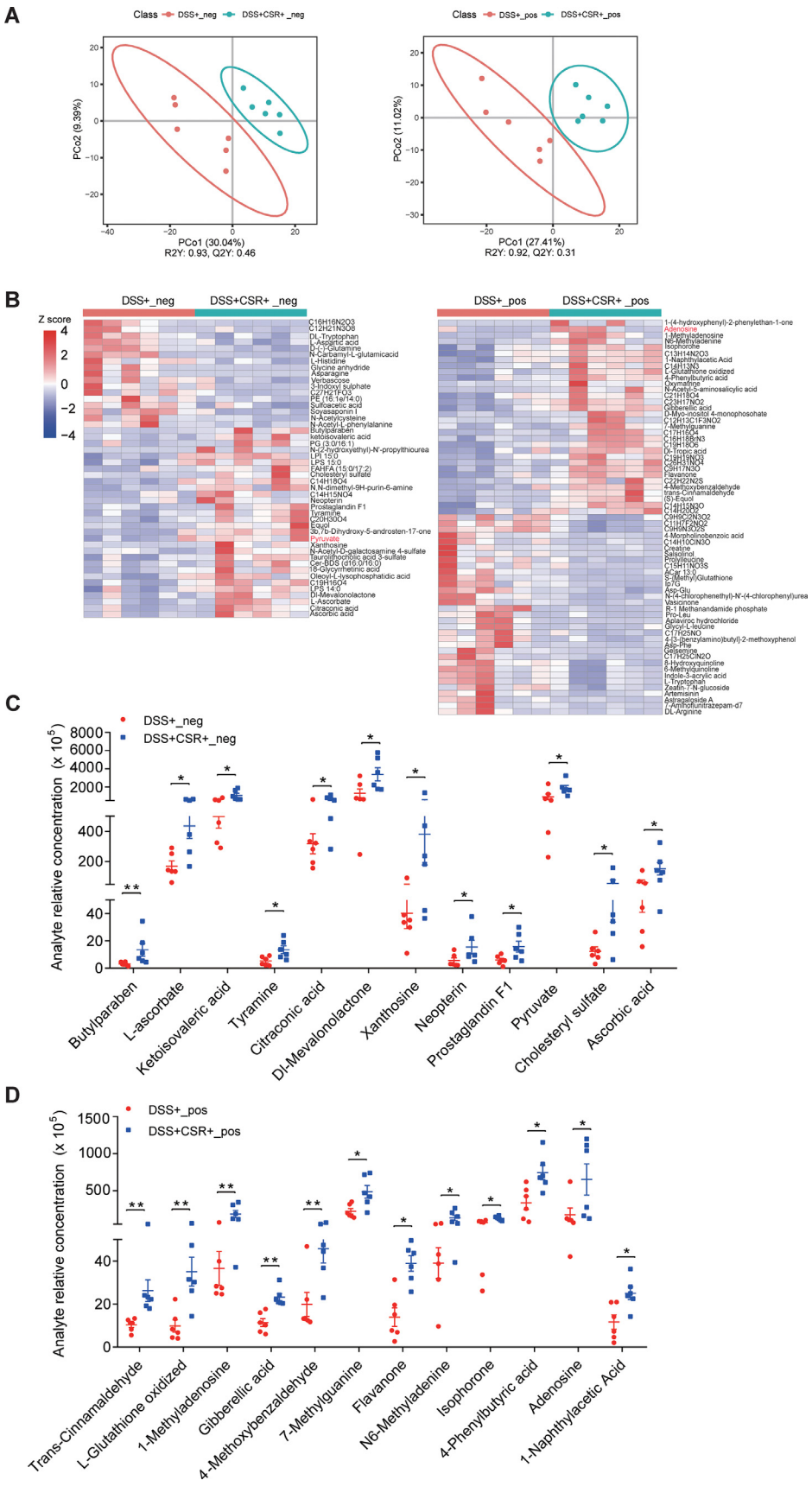
A
Class DSS+_neg DSS+CSR+ _neg
PCo2 (9.39%)
PCo1 (30.04%)
R2Y: 0.93, Q2Y: 0.46
Class DSS+_pos DSS+CSR+_pos
PCo2 (11.02%)
PCo1 (27.41%)
R2Y: 0.92, Q2Y: 0.31
B
DSS+_neg
DSS+CSR+ _neg
Z score
DSS+_pos
DSS+CSR+ _pos
C
DSS+_neg
DSS+CSR+_neg
Analyte relative concentration (x 10^5)
Butylparaben
L-ascorbate
Ketoisovaleric acid
Tyramine
Citraconic acid
Dl-Mevalonolactone
Xanthosine
Neopterin
Prostaglandin F1
Pyruvate
Cholesteryl sulfate
Ascorbic acid
D
DSS+_pos
DSS+CSR+_pos
Analyte relative concentration (x 10^5)
Trans-Cinnamaldehyde
L-Glutathione oxidized
1-Methyladenosine
Gibberellic acid
4-Methoxybenzaldehyde
7-Methylguanine
Flavanone
N6-Methyladenine
Isophorone
4-Phenylbutyric acid
Adenosine
1-Naphthylacetic Acid

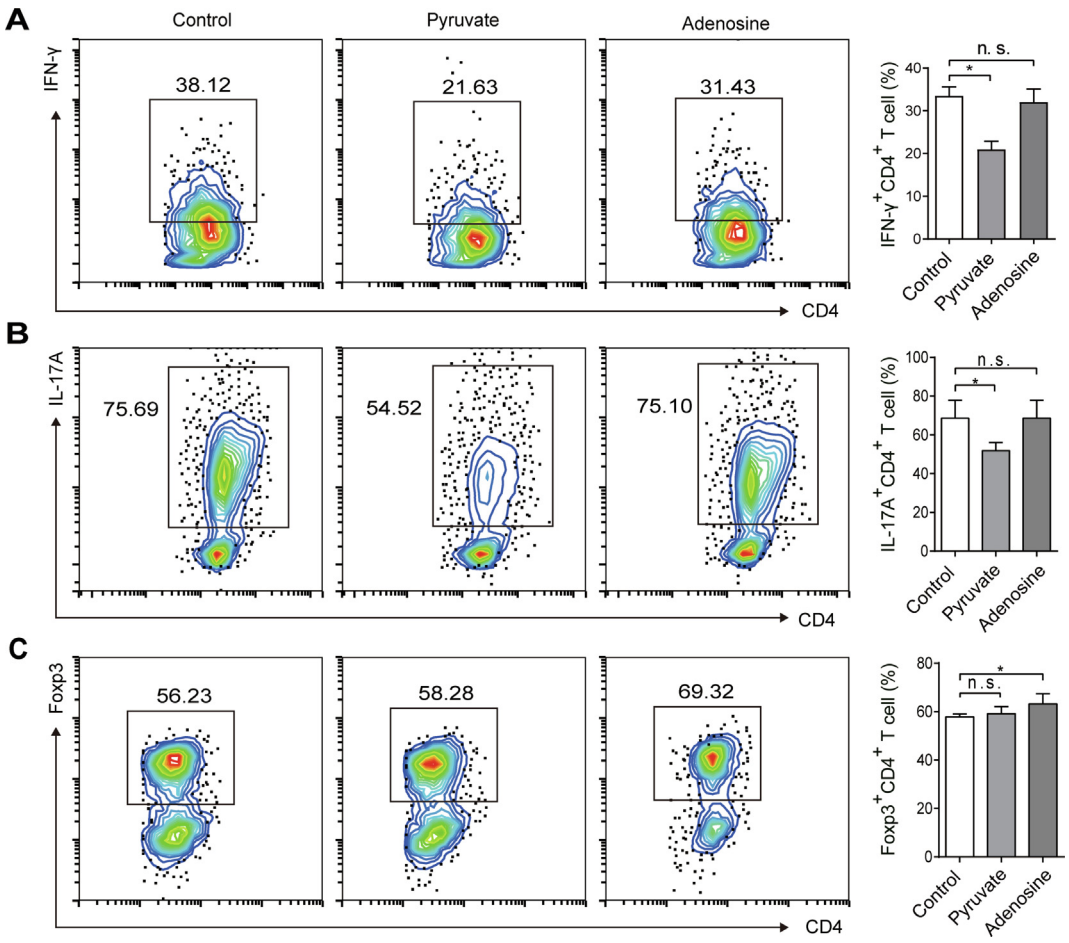

Figure 6 The influence of pyruvate and adenosine treatments on T cell differentiation *in vitro*

Spleen naive $CD4^+$ T cells from C57BL/6 mice were cultured under Th1, Th17, or Treg skewing condition in the presence or absence of pyruvate or adenosine. **A.** IFN-γ^+CD4^+ (Th1) cells from the cotrol, pyruvate-treated, and adenosine-treated groups were analyzed by flow cytometry, and their mean proportions were shown in the bar chart. **B.** IL-$17A^+CD4^+$ (Th17) cells from the cotrol, pyruvate-treated, and adenosine-treated groups were analyzed by flow cytometry, and their mean proportions were shown in the bar chart. **C.** $Foxp3^+CD4^+$ (Treg) cells from the cotrol, pyruvate-treated, and adenosine-treated groups were analyzed by flow cytometry, and their mean proportion were shown in the bar chart. Data were presented as mean ± SEM. The one-way ANOVA with Tukey's test was applied to compare the differences among different groups. *, $P < 0.05$; **, $P < 0.01$; ***, $P < 0.001$; n.s., not significant.

the DSS+CSR+ mice displayed an apparent clustering separation from the DSS+ mice through PCoA, indicating that CSR treatment markedly transforms the biological community structures. Furthermore, the LEfSe analysis among the control, DSS+, and DSS+CSR+ groups revealed that *Odoribacter* and Marinifilaceae were the key types of bacteria in the DSS+ group. Meanwhile, four signature bacterial taxa, including *Prevotellaceae*, *Alloprevotella*, *Paraprevotella*, and *Butyricicoccus*, displayed a relative enrichment in the DSS+CSR+ group. Given that the dysbiosis in patients with IBD is related to the decrease in the number of SCFA/butyrate-producing bacteria [37], the obtained results may indicate a favorable action of CSR on the course of UC. Moreover, the *Prevotellaceae* genus, with the most predominance and the highest LDA score in the DSS+CSR+ group, has been reported to be associated with the remission of IBD [38]. Additionally, *Alloprevotella* has been reported to be related to the decreased lifetime of cardiovascular disease [39], which strengthens the importance of the present findings.

A previous study has illuminated that the metabolites of gut microbiota, such as SCFAs, impose a profound impact on inflammation of IBD [40]. We used untargeted metabolomics

Figure 5 CSR treatment significantly alter gut metabolome

A. PLS-DA of metabolomic profile. **B.** Hierarchical clustering of metabolites. **C.** Relative concentration of metabolites under the negative ion mode in the DSS+ group and DSS+CSR+ group. **D.** Relative concentration of metabolites under the positive ion mode in the DSS+ group and DSS+CSR+ group. Data were pooled in one independent experiment and presented as mean ± SEM. The Student's *t*-test was applied to compare the differences among two groups. *, $P < 0.05$; **, $P < 0.01$; ***, $P < 0.001$. pos, positive; neg, negative; PLS-DA, partial least-squares discrimination analysis.

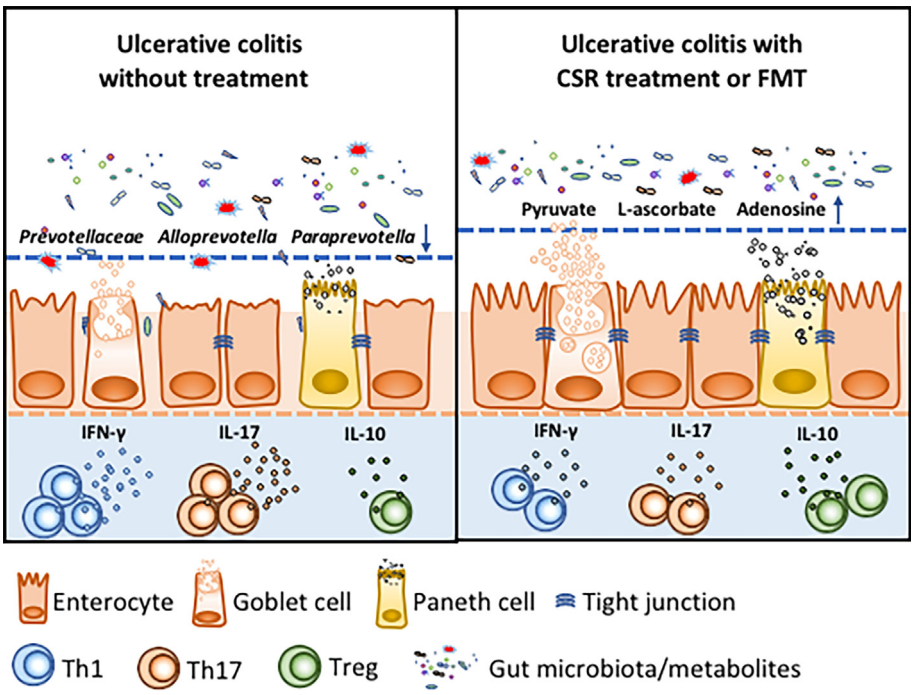

Figure 7 Schematic depicting the protective effects of CSR on DSS-induced colitis

analysis to investigate the potential alteration in metabolome after CSR treatment. The results showed that the concentrations of pyruvate, L-ascorbate, and adenosine were higher in the DSS+CSR+ group. Pyruvate is a key metabolite of microbial cells and the end product of glycolysis, as well as the major metabolite of amino acid and protein metabolism. This acid could prevent hydrogen peroxide-induced apoptosis and enhance the metabolism of fatty acid [41,42]. Fatty acid, with the effects of anti-inflammation and promoting autophagy, is obviously decreased in patients with UC. Moreover, indole-3-pyruvate has also proved to alleviate the inflammation of colon in experimental colitic mice [43]. L-ascorbate could attenuate the production of endotoxin-induced inflammatory mediators by inhibiting mitogen-activated protein kinase (MAPK) activation and NF-κB translocation, and these two signal pathways are activated in IBD [44]. It has also been reported that coordination of ENT2-dependent adenosine transport and signaling could dampen mucosal inflammation [45]. All in all, the up-regulated pyruvate, L-ascorbate, and adenosine might perform their anti-inflammatory effects in a certain way in colitis.

In conclusion, our data demonstrated that CSR ameliorates colon inflammation in a gut microbiota-dependent manner. Although the anti-inflammatory and immunosuppressive properties of CSR have been well described and discussed [25], its effects on the gut microbiota have been not studied. Our study revealed that the underlying protective mechanism of therapeutic action of CSR is associated not only with the rectification of the Treg/Th1 and Treg/Th17 balances and the down-regulation of inflammatory cytokines but also with the modulation of microbiota structure and metabolome. Although the exact role of gut microbiota needs to be further investigated, this study opens up a new direction in the study of traditional medicines.

Materials and methods

Reagents

CSR was purchased from Chem Faces (Catalog No. CFN99198, Wuhan, China).

Animals

Male BALB/c mice (8 weeks old, 18–22 g) were purchased from the Experimental Animal Center of Huazhong University of Science and Technology (Wuhan, China). These animals were socially housed at relatively constant humidity (40%–60%), temperature (22 °C–24 °C), and a 12-h light/dark cycle, and maintained on a normal chow diet with free access to water. All mice were allowed for 1 week housing before the experiment, and then randomly separated into three groups: normal control, DSS+, and DSS+CSR+. The acute experimental colitis model was induced according to a previous study [46]. Briefly, mice in the DSS+CSR+ and DSS+ groups were administrated with 3.0% (W/V) DSS (molecular weight: 36,000–50,000 Da; Catalog No. 160110, MP Biomedicals, Santa Ana, CA) supplemented in filter-purified drinking water for consecutive 7 days, coupled with administration of CSR (1 mg/kg) and equal amount of saline by oral gavage once daily, respectively. Similarly, the normal control group was given distilled water with equal amount of saline by oral gavage once daily. During the DSS treatment, the morbidity, body weight, stool consistency, and stool occult blood of mice were daily monitored. The severity of colitis was measured by DAI score as previously described [47]. The colon length was measured when the mice were euthanized by excessive pentobarbital sodium.

Depletion of the gut microbiota

For the gut microbiota depletion experiment, mice were randomly divided into three groups: ABX+, ABX+DSS+, and ABX+DSS+CSR+. Mice in these three groups were treated with an ABX, including 1 g/l ampicillin (Catalog No. A830931, Macklin, Shanghai, China), 1 g/l neomycin (Catalog No. N6063, Sigma, St. Louis, MO), 1 g/l metronidazole (Catalog No. M813526, Sigma), and 0.5 g/l vancomycin (Catalog No. V871983; Macklin), in drinking water for 3 weeks. Subsequently, the mice in ABX+DSS+ and ABX+DSS+CSR+ groups were treated with 3% DSS in drinking water for consecutive 7 days, coupled with administration of CSR (1 mg/kg) and equal amount of saline by oral gavage once daily, respectively; the mice in the ABX+ group were given distilled water with equal amount of saline by oral gavage once daily for 7 days.

FMT

FMT was performed based on the protocol as previously described [47]. Briefly, donor mice were randomly divided into three groups including the DSS−CSR−, DSS+CSR−, and DSS+CSR+ groups. The DSS+CSR+ and DSS+CSR− groups were treated with DSS diluted in drinking water for consecutive 7 days, coupled with administration of CSR (1 mg/kg) and equal amount of saline by oral gavage once daily, respectively; the DSS−CSR− group was given distilled water with equal amount of saline by oral gavage once daily for 7 days. After the 7-day treatments, the donor mice were housed for another 5 days. Then, the stools from each donor group were collected daily under a laminar flow hood in sterile conditions. Then, the samples were pooled, and 100 mg of the pooled sample was resuspended in 1 ml of sterile saline. The solution was vigorously mixed for 10 s followed by centrifugation at 800 *g* for 3 min. Then, the supernatant was collected and used as transplant material by oral gavage within 10 min to prevent changes in bacterial composition. Recipient mice were randomly divided into three groups. Each group of recipient mice were treated with DSS to induce colitis and simultaneously administrated with 200 μl freshly prepared supernatant per day for 7 days.

Intestinal permeability assay

Intestinal permeability was assessed by the FITC-dextran tracer (molecular weight: 4000 Da; Catalog No. 68059, Sigma). Mice were fasted overnight and then administered with 0.5 ml FITC-dextran by oral gavage 4 h before being euthanized. Then, blood samples were collected when mice were euthanized, and the samples were centrifuged at 6000 *g* for 90 s. Concentration of FITC-dextran was determined using fluorescence spectrometry at the excitation wavelength of 488 nm and the emission wavelength of 520 nm within 5 min [48].

Histopathology and Alcian blue staining

The colons were emptied of fecal contents, opened longitudinally along the mesenteric border, formed a Swiss-Roll from the proximal to the distal end, and then placed in 4% paraformaldehyde for 24 h. The Swiss-Rolls were transferred to paraffin-embedded blocks to generate 5-μm-thick sections for H&E staining followed by blind assessment by a pathologist. The 5-μm-thick sections were also stained with Alcian blue periodic acid following the standard protocol. Slices were visualized under a light microscope (Catalog No. GSL-10/GSL-120/MB8, Leica, Weztlar, Germany).

Mouse colonic LPL isolation

Mouse colons were opened longitudinally and washed with cold phosphate-buffered saline (PBS) supplemented with 1 M Hepes to remove the fecal contents. Pooled colons were cut into 0.5-cm pieces and washed with 25 ml of hank's balanced salt solution (HBSS; Catalog No. C14175500BT, Gibco, Grand Island, NY) containing 1 M Hepes and 500 mM ethylene diamine tetraacetic acid (EDTA) on an orbital shaker at 100 r/min for 25 min at 37 °C. Then, the colon pieces were washed twice using cold PBS supplemented with 1 M Hepes. After washing, the colons were finely cut and digested with 10 ml Roswell Park Memorial Institute (RPMI) 1640 (Catalog No. 11875-119, Gibco) containing 1 mg/ml DNase I (Catalog No. 10104159001, Roche, Mannheim, Germany) and 0.5 mg/ml Type-D Collagenase (Catalog No. 11088858001, Roche) on an orbital shaker at 100 r/min for 15 min at 37 °C. After digestion, the colonic LPL cells were filtered through 100-μm strainer, centrifuged at 1650 r/min for 5 min at 4 °C, and finally resuspended in 500 μl PBS for flow cytometric analysis [49].

Flow cytometry

Flow cytometry was performed as described previously [50]. Briefly, single-cell suspensions were stained with indicated antibodies diluted by PBS supplemented with 2% fetal bovine serum (FBS) and 0.5% bovine serum albumin (BSA) for surface markers. For the staining of intracellular cytokines IFN-γ and IL-17A, cells were incubated and stimulated with 200 ng/ml phorbol myristate acetate (PMA) (Catalog No. BML-PE160-0005, Enzo, Farmingdale, NY), 1 μg/ml ionomycin (Catalog No. ALX-450-007-M001, Enzo), and 1 μg/ml brefeldin A (Catalog No. 00-4506-51, eBioscience, Carlsbad, CA) at 37 °C for 6 h. Then, the cultured cells were collected, washed, stained for surface markers CD45 and CD4 for 20 min, fixed and permeabilized with fixation and permeabilization buffer (Catalog No. 88-8824-00, ThermoFisher Scientific, Waltham, MA) at room temperature for 30 min, and then stained intracellularly with anti-IFN-γ and anti-IL-17A antibodies for 30 min. For Foxp3, T-bet, and ROR-γt staining, the cells were stained for surface markers such as CD45 and CD4, followed by fixation and permeabilization with fixation and permeabilization buffer (Catalog No. 88-8824-00, ThermoFisher Scientific) at room temperature for 30 min. After washes, the cells were then stained with anti-Foxp3, anti-T-bet, or anti-ROR-γt antibody as instructed. All samples were detected by flow cytometry (CytoFLEX LX, Beckman Coulter, Pasadena, CA) and analyzed with the CytExpert 2.0 software. Antibodies used for flow cytometry included anti-mouse CD45-FITC (Catalog No. 553080, BD Biosciences, Franklin Lakes, NJ), CD4-PE/Cy7 (Catalog No. 552775, BD Biosciences), IL-17A-PE (Catalog No. 561020, BD Biosciences), IFN-γ-APC (Catalog No. 562018, BD Biosciences), ROR-γt-BV421 (Catalog No. 562894, BD Biosciences), Foxp3-PE (Catalog No. 12-5773-82, ThermoFisher Scientific),

T-bet-APC (Catalog No. 561264, BD Biosciences), and Fixable Viability Stain 510 (Catalog No. 564406, BD Biosciences). Flow gating strategies for each cell population are shown in Figure S9.

qRT-PCR

Total RNA was extracted from colonic tissues using RNAiso Plus (Catalog No. 9109, TaKaRa, Dalian, China) according to the manufacturer's protocols. Then, cDNA was synthesized using PrimeScript RT Master Mix (Catalog No. RR036A, TaKaRa), and analyzed to explore gene expression changes using SYBR Premix Ex Taq (Catalog No. RR420A, TaKaRa). The relative expression levels of genes in tissues were normalized to *ACTB*. The sequences of all primers are listed in Table S1.

Immunohistochemistry

Colonic tissues were fixed, paraffin-embedded, and sectioned (4 μm). The deparaffinized and rehydrated sections were subjected to antigen retrieval using sodium citrate buffer. After incubation with 10% normal goat serum (Catalog No. WGAR1009-5, Servicebio, Wuhan, China) for 1 h, the sections were incubated with primary antibody overnight at 4 °C. Antibodies used for flow cytometry included anti-mouse Occludin (Catalog No. DF7504, Affinity, Liyang, China), Zo-1 (Catalog No. AF5145, Affinity), Claudin-2 (Catalog No. AF0128, Affinity), IFN-γ (Catalog No. DF6045, Affinity), TNF-α (Catalog No. AF7014, Affinity). The subsequent procedures were performed according to the manufacturer's instructions.

Fecal genomic DNA extraction and 16S rRNA sequencing

The mice used for gut microbiota sequencing were age-matched litter mates. Fecal genomic DNA extraction and 16S rRNA sequencing were performed at Novogene (Beijing, China). Total genome DNA from fecal samples was extracted using the hexadecyltrimethylammonium bromide/sodium dodecyl sulfate (CTAB/SDS) method. Concentration and purity of DNA were monitored on 1% agarose gels. According to the concentration, DNA was diluted into 1 ng/μl using sterile water. The V3–V4 variable regions of the16S rRNA genes were amplified using specific primers with the barcode. All PCR reactions were carried out using Phusion High-Fidelity PCR Master Mix (Catalog No. M0531S, New England Biolabs, Lpswich, MA). The PCR products were then mixed with the same volume of 1× loading buffer (containing SYBR green) and detected by electrophoresis on 2% agarose gel. Different PCR products were mixed in equidensity ratios. Then, mixed PCR products were purified with GeneJET Gel Extraction Kit (Catalog No. K0691, ThermoFisher Scientific). Sequencing libraries were generated using Ion Plus Fragment Library Kit 48 rxns (Catalog No. 4471252, ThermoFisher Scientific) following manufacturer's recommendations. The library quality was assessed on the Qubit 2.0 Fluorometer (ThermoFisher Scientific). At last, the library was sequenced on an Ion S5 XL platform and 600 bp single-end reads were generated.

Untargeted metabolomics analysis

Untargeted metabolomics analysis was performed at Novogene (Beijing, China). Fecal samples (100 mg) were individually grounded with liquid nitrogen and the homogenate was resuspended with prechilled 80% methanol and 0.1% formic acid by fully vortexing. The samples were incubated on ice for 5 min and then were centrifuged at 15,000 r/min for 5 min at 4 °C. And then, the supernatant was diluted to a final concentration containing 53% methanol by liquid chromatograph mass spectrometer (LC–MS) grade water. The samples were subsequently transferred to a fresh Eppendorf tube and then were centrifuged at 15,000 *g* for 10 min at 4 °C for 10 min. Finally, the supernatant was injected into the LC–MS system for analysis. LC–MS analysis was performed using a Vanquish ultra-high-performance liquid chromatography (UHPLC) system (ThermoFisher Scientific) coupled with an Q Exactive Orbitrap series mass spectrometer (ThermoFisher Scientific). The raw data files generated by UHPLC–MS were processed using the Compound Discoverer 3.1 (ThermoFisher Scientific) to perform peak alignment, peak picking, and quantitation for each metabolite. Then, these metabolites were annotated using the Kyoto Encyclopedia of Genes and Genomes (KEGG) database, the human metabolome database (HMDB), and the Lipidmaps database. PCoA, PLS-DA, Volcano plots, and clustering heatmaps were performed to show the relationship of metabolites between two groups.

Isolation of naive $CD4^+$ T cells and *in vitro* induction of differentiation

Total spleen T cells were purified by negative selection using the mouse Naive $CD4^+$ T Cell Isolation Kit (Catalog No. 130-104-453, Miltenyi Biotec, Bergisch Gladbach, Germany) and LS separation columns (Catalog No. 130-042-401, Miltenyi Biotec) following the manufacturer's instructions. Naive $CD4^+$ T cells were seeded in 96-well plates coated with anti-CD3 (Catalog No. 16-0032-85, ThermoFisher Scientific) and anti-CD28 (Catalog No. 16-0281-85, ThermoFisher Scientific) antibodies at 2×10^5 cells/well in RPMI 1640 medium (Catalog No. 11875-119, Gibco) containing 10% inactivated FBS (Catalog No. 10099141, Gibco).

For Th1 cell differentiation, naive $CD4^+$ T cells were cultured with 10 ng/ml IL-12 (Catalog No. 402-ML-020/CF, R&D, Minneapolis, MN) and 10 μg/ml anti-IL-4 (Catalog No. BE0045, Bio X Cell, West Lebanon, NH). For Th17 cell differentiation, naive $CD4^+$ T cells were cultured with 2 ng/ml TGF-β (Catalog No. 240-B-002/CF, R&D), 10 ng/ml IL-6 (Catalog No. 406-ML-005/CF, R&D), 10 μg/ml anti-IFN-γ (Catalog No. BE0055, Bio X Cell), 10 μg/ml anti-IL-4 (Catalog No. BE0045, Bio X Cell), and 10 μg/ml anti-IL-2 (Catalog No. BE0043-1, Bio X Cell). For Treg cell differentiation, naive $CD4^+$ T cells were cultured with 2 ng/ml TGF-β (Catalog No. 240-B-002/CF, R&D).

The effects of different concentrations of CSR, pyruvate (Catalog No. P6033, Macklin), and adenosine (Catalog No. A6218, Macklin) on the differentiation of Th1, Th17, and Treg were assessed by flow cytometry after 72 h culture.

Statistical analysis

All experiments adopted randomization and blind data analyses, and were designed to generate groups of equal size. In any experiment, no data points were excluded from the analysis.

The data of qRT-PCR were normalized to control to avoid unwanted sources of variation. The statistical analysis was undertaken only for studies where each group size was at least n = 5. Data were presented as mean ± standard error of the mean (SEM), and statistical analysis was performed using GraphPad Prism (GraphPad Prism version 6.0). Student's *t*-test was used to compare the means of two groups. And comparisons among multiple groups were performed with one-way analysis of variance (ANOVA) with Tukey's test. Post hoc test was run only when F reaches $P < 0.05$, and the variance inhomogeneity is not significant. $P < 0.05$ was considered statistically significant. The declare group size was the number of independent values, and statistical analysis was performed using these independent values (technical replicates were not treated as independent values).

Ethical statement

All animal care and experimental procedures were approved by the Committee for Animal Research of Huazhong University of Science and Technology (Wuhan, China) (No. IACUC-2532).

Data availability

The 16S rRNA sequencing data have been submitted to the Genome Sequence Archive [51] at the National Genomics Data Center, Beijing Institute of Genomics, Chinese Academy of Sciences / China National Center for Bioinformation (GSA: CRA005121), and are publicly accessible at https://ngdc.cncb.ac.cn/gsa.

CRediT author statement

Mingyue Li: Conceptualization, Formal analysis, Methodology, Investigation, Software, Writing - original draft, Writing - review & editing. **Weina Guo:** Validation, Writing - review & editing. **Yalan Dong:** Conceptualization, Formal analysis, Methodology, Investigation, Software, Writing - original draft, Writing - review & editing. **Wenzhu Wang:** Validation, Writing - review & editing. **Chunxia Tian:** Investigation. **Zili Zhang:** Validation, Software. **Ting Yu:** Validation. **Haifeng Zhou:** Methodology. **Yang Gui:** Investigation, Formal analysis. **Kaming Xue:** Data curation. **Junyi Li:** Methodology, Funding acquisition. **Feng Jiang:** Data curation. **Alexey Sarapultsev:** Methodology. **Huafang Wang:** Writing - review & editing. **Ge Zhang:** Writing - review & editing. **Shanshan Luo:** Supervision. **Heng Fan:** Project administration. **Desheng Hu:** Funding acquisition, Project administration, Supervision, Writing - review & editing. All authors have read and approved the final manuscript.

Competing interests

The authors have declared no competing interests.

Acknowledgments

This study was funded by the grants from the National Key R&D Program of China (Grant No. 2019YFC1316204), the National Natural Science Foundation of China (Grant Nos. 81974249, 31770983, 82070136, and 82104488), and the Hubei Provincial Natural Science Foundation of China (Grant No. 2020BHB016).

Supplementary material

Supplementary data to this article can be found online at https://doi.org/10.1016/j.gpb.2022.05.002.

ORCID

ORCID 0000-0003-4207-8917 (Mingyue Li)
ORCID 0000-0002-7494-5416 (Weina Guo)
ORCID 0000-0002-1065-5962 (Yalan Dong)
ORCID 0000-0001-6066-5053 (Wenzhu Wang)
ORCID 0000-0002-0745-1459 (Chunxia Tian)
ORCID 0000-0002-0383-7303 (Zili Zhang)
ORCID 0000-0002-4482-4314 (Ting Yu)
ORCID 0000-0002-7564-5087 (Haifeng Zhou)
ORCID 0000-0001-9981-1046 (Yang Gui)
ORCID 0000-0002-3379-4148 (Kaming Xue)
ORCID 0000-0003-2599-2889 (Junyi Li)
ORCID 0000-0002-2476-1918 (Feng Jiang)
ORCID 0000-0003-3101-9655 (Alexey Sarapultsev)
ORCID 0000-0001-6226-072X (Huafang Wang)
ORCID 0000-0002-7807-7695 (Ge Zhang)
ORCID 0000-0002-0961-4215 (Shanshan Luo)
ORCID 0000-0002-1100-0757 (Heng Fan)
ORCID 0000-0002-9608-0310 (Desheng Hu)

References

[1] Kaplan GG, Ng SC. Understanding and preventing the global increase of inflammatory bowel disease. Gastroenterology 2017;152:313–21.
[2] Ng SC, Shi HY, Hamidi N, Underwood FE, Tang W, Benchimol EI, et al. Worldwide incidence and prevalence of inflammatory bowel disease in the 21st century: a systematic review of population-based studies. Lancet 2018;390:2769–78.
[3] Harbord M, Eliakim R, Bettenworth D, Karmiris K, Katsanos K, Kopylov U, et al. Third European evidence-based consensus on diagnosis and management of ulcerative colitis. Part 2: current management. J Crohns Colitis 2017;11:769–84.
[4] Rubin DT, Ananthakrishnan AN, Siegel CA, Sauer BG, Long MD. ACG clinical guideline: ulcerative colitis in adults. Am J Gastroenterol 2019;114:384–413.
[5] Kobayashi T, Siegmund B, Le Berre C, Wei SC, Ferrante M, Shen B, et al. Ulcerative colitis. Nat Rev Dis Primers 2020;6:73.
[6] Kaser A, Zeissig S, Blumberg RS. Inflammatory bowel disease. Annu Rev Immunol 2010;28:573–621.
[7] Himmel ME, Hardenberg G, Piccirillo CA, Steiner TS, Levings MK. The role of T-regulatory cells and Toll-like receptors in the pathogenesis of human inflammatory bowel disease. Immunology 2008;125:145–53.
[8] Bedoya SK, Lam B, Lau K, Larkin J. Th17 cells in immunity and autoimmunity. Clin Dev Immunol 2013;2013:986789.
[9] Benedetti G, Miossec P. Interleukin 17 contributes to the chronicity of inflammatory diseases such as rheumatoid arthritis. Eur J Immunol 2014;44:339–47.
[10] Brand S. Crohn's disease: Th1, Th17 or both? The change of a paradigm: new immunological and genetic insights implicate Th17 cells in the pathogenesis of Crohn's disease. Gut 2009;58:1152–67.

[11] Luo A, Leach ST, Barres R, Hesson LB, Grimm MC, Simar D. The microbiota and epigenetic regulation of T helper 17/regulatory T cells: in search of a balanced immune system. Front Immunol 2017;8:417.
[12] Tillack C, Ehmann LM, Friedrich M, Laubender RP, Papay P, Vogelsang H, et al. Anti-TNF antibody-induced psoriasiform skin lesions in patients with inflammatory bowel disease are characterised by interferon-γ-expressing Th1 cells and IL-17A/IL-22-expressing Th17 cells and respond to anti-IL-12/IL-23 antibody treatment. Gut 2014;63:567–77.
[13] Wang X, Ma C, Wu J, Zhu J. Roles of T helper 17 cells and interleukin-17 in neuroautoimmune diseases with emphasis on multiple sclerosis and Guillain-Barré syndrome as well as their animal models. J Neurosci Res 2013;91:871–81.
[14] Lavelle A, Sokol H. Gut microbiota-derived metabolites as key actors in inflammatory bowel disease. Nat Rev Gastroenterol Hepatol 2020;17:223–37.
[15] Britton GJ, Contijoch EJ, Mogno I, Vennaro OH, Llewellyn SR, Ng R, et al. Microbiotas from humans with inflammatory bowel disease alter the balance of gut Th17 and RORγt$^+$ regulatory T cells and exacerbate colitis in mice. Immunity 2019;50:212–24.
[16] Krishnan S, Ding Y, Saedi N, Choi M, Sridharan GV, Sherr DH, et al. Gut microbiota-derived tryptophan metabolites modulate inflammatory response in hepatocytes and macrophages. Cell Rep 2018;23:1099–111.
[17] Del Rio D, Zimetti F, Caffarra P, Tassotti M, Bernini F, Brighenti F, et al. The gut microbial metabolite trimethylamine-*N*-oxide is present in human cerebrospinal fluid. Nutrients 2017;9:1053.
[18] Smith PM, Howitt MR, Panikov N, Michaud M, Gallini CA, Bohlooly-Y M, et al. The microbial metabolites, short-chain fatty acids, regulate colonic Treg cell homeostasis. Science 2013;341:569–73.
[19] Inagaki T, Moschetta A, Lee YK, Peng L, Zhao G, Downes M, et al. Regulation of peptidecterial defense in the small intestine by the nuclear bile acid receptor. Proc Natl Acad Sci U S A 2006;103:3920–5.
[20] D'Aldebert E, Biyeyeme Bi Mve MJ, Mergey M, Wendum D, Firrincieli D, Coilly A, et al. Bile salts control the antimicrobial peptide cathelicidin through nuclear receptors in the human biliary epithelium. Gastroenterology 2009;136:1435–43.
[21] Zenewicz LA, Yancopoulos GD, Valenzuela DM, Murphy AJ, Stevens S, Flavell RA. Innate and adaptive interleukin-22 protects mice from inflammatory bowel disease. Immunity 2008;29:947–57.
[22] Li Y, Innocentin S, Withers DR, Roberts NA, Gallagher AR, Grigorieva EF, et al. Exogenous stimuli maintain intraepithelial lymphocytes via aryl hydrocarbon receptor activation. Cell 2011;147:629–40.
[23] Cascao R, Fonseca JE, Moita LF. Celastrol: a spectrum of treatment opportunities in chronic diseases. Front Med (Lausanne) 2017;4:69.
[24] Shaker ME, Ashamallah SA, Houssen ME. Celastrol ameliorates murine colitis via modulating oxidative stress, inflammatory cytokines and intestinal homeostasis. Chem Biol Interact 2014;210:26–33.
[25] Jia Z, Xu C, Shen J, Xia T, Yang J, He Y. The natural compound celastrol inhibits necroptosis and alleviates ulcerative colitis in mice. Int Immunopharmacol 2015;29:552–9.
[26] Croswell A, Amir E, Teggatz P, Barman M, Salzman NH. Prolonged impact of antibiotics on intestinal microbial ecology and susceptibility to enteric *Salmonella* infection. Infect Immun 2009;77:2741–53.
[27] Yang W, Cong Y. Gut microbiota-derived metabolites in the regulation of host immune responses and immune-related inflammatory diseases. Cell Mol Immunol 2021;18:866–77.
[28] Chassaing B, Aitken JD, Malleshappa M, Vijay-Kumar M. Dextran sulfate sodium (DSS)-induced colitis in mice. Curr Protoc Immunol 2014;104:15.25.1–14.
[29] Taghipour N, Molaei M, Mosaffa N, Rostami-Nejad M, Aghdaei HA, Anissian A, et al. An experimental model of colitis induced by dextran sulfate sodium from acute progresses to chronicity in C57BL/6: correlation between conditions of mice and the environment. Gastroenterol Hepatol Bed Bench 2016;9:45–52.
[30] Venkatesha SH, Moudgil KD. Celastrol suppresses experimental autoimmune encephalomyelitis via MAPK/SGK1-regulated mediators of autoimmune pathology. Inflamm Res 2019;68:285–96.
[31] Astry B, Venkatesha SH, Laurence A, Christensen-Quick A, Garzino-Demo A, Frieman MB, et al. Celastrol, a Chinese herbal compound, controls autoimmune inflammation by altering the balance of pathogenic and regulatory T cells in the target organ. Clin Immunol 2015;157:228–38.
[32] Hold GL, Smith M, Grange C, Watt ER, El-Omar EM, Mukhopadhya I. Role of the gut microbiota in inflammatory bowel disease pathogenesis: what have we learnt in the past 10 years? World J Gastroenterol 2014;20:1192–210.
[33] Tremaroli V, Bäckhed F. Functional interactions between the gut microbiota and host metabolism. Nature 2012;489:242–329.
[34] Gionchetti P, Rizzello F, Venturi A, Brigidi P, Matteuzzi D, Bazzocchi G, et al. Oral bacteriotherapy as maintenance treatment in patients with chronic pouchitis: a double-blind, placebo-controlled trial. Gastroenterology 2000;119:305–9.
[35] Grimm V, Riedel CU. Manipulation of the microbiota using probiotics. Adv Exp Med Biol 2016;902:109–17.
[36] Haifer C, Leong RW, Paramsothy S. The role of faecal microbiota transplantation in the treatment of inflammatory bowel disease. Curr Opin Pharmacol 2020;55:8–16.
[37] Venegas DP, De la Fuente MK, Landskron G, Gonzalez MJ, Quera R, Dijkstra G, et al. Short chain fatty acids (SCFAs)-mediated gut epithelial and immune regulation and its relevance for inflammatory bowel diseases. Front Immunol 2019;10:277.
[38] Huang K, Dong W, Liu W, Yan Y, Wan P, Peng Y, et al. 2-*O*-β-D-Glucopyranosyl-L-ascorbic acid, an ascorbic acid derivative isolated from the fruits of *Lycium barbarum* L., modulates gut microbiota and palliates colitis in dextran sodium sulfate-induced colitis in mice. J Agric Food Chem 2019;67:11408–19.
[39] Kelly TN, Bazzano LA, Ajami NJ, He H, Zhao J, Petrosino JF, et al. Gut microbiome associates with lifetime cardiovascular disease risk profile among bogalusa heart study participants. Circ Res 2016;119:956–64.
[40] Huda-Faujan N, Abdulamir AS, Fatimah AB, Anas OM, Shuhaimi M, Yazid AM, et al. The impact of the level of the intestinal short chain fatty acids in inflammatory bowel disease patients *versus* healthy subjects. Open Biochem J 2010;4:53–8.
[41] Kamzolova SV, Morgunov IG. Biosynthesis of pyruvic acid from glucose by *Blastobotrys adeninivorans*. Appl Microbiol Biotechnol 2016;100:7689–97.
[42] Ramakrishnan N, Chen R, McClain DE, Bünger R. Pyruvate prevents hydrogen peroxide-induced apoptosis. Free Radic Res 1998;29:283–95.
[43] Aoki R, Aoki-Yoshida A, Suzuki C, Takayama Y. Indole-3-pyruvic acid, an aryl hydrocarbon receptor activator, suppresses experimental colitis in mice. J Immunol 2018;201:3683–93.
[44] Huang YN, Lai CC, Chiu CT, Lin JJ, Wang JY. L-ascorbate attenuates the endotoxin-induced production of inflammatory mediators by inhibiting MAPK activation and NF-κB translocation in cortical neurons/glia Cocultures. PLoS One 2014;9:e97276.
[45] Aherne CM, Collins CB, Rapp CR, Olli KE, Perrenoud L, Jedlicka P, et al. Coordination of ENT2-dependent adenosine transport and signaling dampens mucosal inflammation. JCI Insight 2018;3:e121521.
[46] Wirtz S, Popp V, Kindermann M, Gerlach K, Weigmann B, Fichtner-Feigl S, et al. Chemically induced mouse models of acute and chronic intestinal inflammation. Nat Protoc 2017;12:1295–309.
[47] Yang J, Liu XX, Fan H, Tang Q, Shou ZX, Zuo DM, et al. Extracellular vesicles derived from bone marrow mesenchymal

stem cells protect against experimental colitis via attenuating colon inflammation, oxidative stress and apoptosis. PLoS One 2015;10:e0140551.

[48] Ma X, Sun Q, Sun X, Chen D, Wei C, Yu X, et al. Activation of $GABA_A$ receptors in colon epithelium exacerbates acute colitis. Front Immunol 2018;9:987.

[49] Ivanov II, McKenzie BS, Zhou L, Tadokoro CE, Lepelley A, Lafaille JJ, et al. The orphan nuclear receptor RORγt directs the differentiation program of proinflammatory IL-17^+ T helper cells. Cell 2006;126:1121–33.

[50] Ji J, Ge X, Chen Y, Zhu B, Wu Q, Zhang J, et al. Daphnetin ameliorates experimental colitis by modulating microbiota composition and Treg/Th17 balance. FASEB J 2019;33:9308–22.

[51] Chen T, Chen X, Zhang S, Zhu J, Tang B, Wang A, et al. The Genome Sequence Archive Family: toward explosive data growth and diverse data types. Genomics Proteomics Bioinformatics 2021;19:578–83.